into the mantle. The shear of the upwelling may be a consequence of the migration of the African plate to the northeast since the breakup of Gondwanaland, interaction with midmantle heterogeneity, the 670-km phase transition or a putative physical boundary near 2000 km depth (*3*, *29*).

The weakening of the low velocity anomaly between 670 and 1000 km depth indicates that the upwelling is obstructed. Eventually, however, an upwelling may form in the transition zone beneath eastern Africa, which propagates along the base of the lithosphere into the East African rift region. The central location of the upwelling in the deep mantle beneath southern Africa can explain the anomalously high elevation of southern Africa and of its contiguous ocean basins and the high long-wavelength geoid over Africa and the Atlantic Ocean (*17*). The continuity of this upwelling into the upper mantle region beneath East Africa compels a link between a relatively hot CMB region and flood basalt volcanism that formed the Ethiopian traps and contributed to the rifting in the Red Sea, the Gulf of Aden, and along the East African Rift (*30*).

References and Notes

1. A. M. Dziewonski, *J. Geophys. Res.* **89**, 5929 (1984).
2. J. H. Woodhouse and A. M. Dziewonski, *J. Geophys. Res.* **89**, 5953 (1984).
3. W.-S. Su, R. L. Woodward, A. M. Dziewonski, *J. Geophys. Res.* **99**, 6945 (1994).
4. G. Masters, S. Johnson, G. Laske, H. Bolton, *Philos. Trans. R. Soc. London A.* **354**, 1385 (1996).
5. X.-D. Li and B. Romanowicz, *J. Geophys. Res.* **101**, 22,245 (1996).
6. X.-F. Liu and A. M. Dziewonski, in *The Core-Mantle Boundary Region*, M. Gurnis, M. E. Wysession, E. Knittle, B. A. Buffet, Eds. (American Geophysical Union, Washington, DC, 1998), pp. 21-36.
7. S. P. Grand, R. D. Van der Hilst, S. Widiyantoro, *Geol. Soc. Am. Today* **7**, 1 (1997).
8. H. Bijwaard, W. Spakman, E. R. Engdahl, *J. Geophys. Res.* **103**, 30,055 (1998).
9. Reviews of the fate of subducting slabs are given in P. Silver, R. W. Carlson, P. Olson, *Annu. Rev. Earth Planet. Sci.* **16**, 477 (1988), and T. Lay, *Annu. Rev. Earth Planet. Sci.* **22**, 33 (1994).
10. D. Bercovici and J. Mahoney, *Science* **26**, 1367 (1994).
11. C. Kincaid, G. Ito, C. Gable, *Nature* **376**, 758 (1995).
12. T. Nakakuki, H. Sato, H. Fujimoto, *Earth Planet. Sci. Lett.* **121**, 369 (1994).
13. D. A. Yuen, L. Cserepes, B. A. Schroeder, *Earth Planets Space* **50**, 1035 (1998).
14. H.-C. Nataf and J. C. VanDecar, *Nature* **364**, 115 (1993).
15. H. J. Van Heijst, J. Ritsema, J. H. Woodhouse, *Eos* (spring suppl.) **80**, S221 (1999).
16. W. J. Morgan, *Nature* **230**, 42 (1971); M. A. Richards, B. H. Hager, N. H. Sleep, *J. Geophys. Res.* **93**, 7690 (1988); C. J. Ebinger and N. H. Sleep, *Nature* **395**, 788 (1998).
17. B. H. Hager *et al.*, *Nature* **313**, 541 (1985); A. A. Nyblade and S. W. Robinson, *Geophys. Res. Lett.* **21**, 765 (1994); C. Lithgow-Bertelloni and P. G. Silver, *Nature* **395**, 269 (1998).
18. T. Lay, Q. Williams, E. J. Garnero, *Nature* **392**, 461 (1998).
19. Phase velocity of fundamental mode and up to the fourth overtone Rayleigh waves are determined using the Mode Branch stripping technique [H. J. Van Heijst and J. H. Woodhouse, *Geophys. J. Int.* **131**, 209 (1997)], involving cross-correlation of single-mode branch synthetics with long-period seismograms. Phase velocity maps of these fundamental and overtone Rayleigh wave data are presented in H. J. Van Heijst and J. H. Woodhouse [*Geophys. J. Int.* **137**, 601 (1999)].
20. Travel times are estimated by cross-correlating observed waveforms with normal mode synthetics, computed for the PREM (22) and Harvard Centroid Moment Tensor source parameters [A. M. Dziewonski, T.-A. Chou, J. H. Woodhouse, *J. Geophys. Res.* **86**, 2825 (1981)]. The waveforms are low-pass filtered at periods >15 s to reduce the effects of complex earthquake rupture processes and to increase signal-to-noise ratio. The exact waveform synthesis by normal mode summation facilitates the analysis of seismic phases with emergent onsets (for example, *SS*, *SKKS*, and S_{diff}) and small-amplitude phases (for example, *SSS* and ScS_2) recorded after the high-amplitude first arrivals.
21. The normal mode data used in this report are compiled by J. S. Resovsky and M. H. Ritzwoller [*J. Geophys. Res.* **104**, 993 (1999)] and have been retrieved from http://tagg.colorado.edu/geophysics/nm./dir/ of the University of Colorado.
22. A. M. Dziewonski and D. L. Anderson, *Phys. Earth Plan. Inter.* **25**, 297 (1981).
23. We account for the effects of topography and crustal thickness variation using the model CRUST5.1 [W. D. Mooney, G. Laske, G. Masters, *J. Geophys. Res.* **103**, 727 (1998)]. Seismic velocity variations are parameterized using 21 vertical spline functions and spherical harmonics up to degree 20. The inversion involves two steps: earthquake source relocation, and damped least-squares inversion for shear velocity structure. We iterate upon these steps until maximum variance reduction is obtained. The damped least-squares inversion for model parameters involves the computation of the eigenvalue decomposition, allowing us to determine model resolution. We do not apply smoothness constraints to the model.
24. Y. Shen, S. C. Solomon, I. Th. Bjarnason, C. J. Wolfe, *Nature* **395**, 62 (1998).
25. H. Bijwaard and W. Spakman, *Earth Planet Sci. Lett.* **166**, 121 (1999).
26. G. E. Backus and J. F. Gilbert, *Geophys. J. R. Astron. Soc.* **16**, 169 (1968). A Backus-Gilbert kernel $R(r_0, r)$ describes how the shear wave velocity $V_s^m(r_0)$ in the model at r_0 is a spatial average of shear wave velocity in the actual Earth: $V_s^m(r_0) = \int_V R(r_0, r) V_s(r)dr$. If resolution is perfect, Backus-Gilbert kernels are delta-functions $\delta(r_0 - r)$. However, they are typically less localized due to the finite number of model parameters, limited data coverage, and model norm damping.
27. U. Christensen, *Ann. Geophys.* **2**, 311 (1984); P. J. Tackley, in *The Core-Mantle Boundary Region*, M. Gurnis, M. E. Wysession, E. Knittle, B. A. Buffet, Eds. (American Geophysical Union, Washington, DC, 1998), pp. 231–253; M. Ishii and J. Tromp, *Science* **285**, 1231 (1999).
28. S. Zhong and M. Gurnis, *J. Geophys. Res.* **98**, 12,219 (1993).
29. L. H. Kellogg, B. H. Hager, R. D. Van der Hilst, *Science* **283**, 1881 (1999).
30. C. Hofmann *et al.*, *Nature* **389**, 838 (1997); I. Manighetti *et al.*, *J. Geophys. Res.* **102**, 2681 (1997); C. Prodehl *et al.* *Tectonophysics* **278**, 121 (1997); C. J. Ebinger and N. H. Sleep, *Nature* **395**, 788 (1998); V. Courtillot *et al.*, *Earth Planet. Sci. Lett.* **166**, 177 (1999).

31. Data were provided by the IRIS and GEOSCOPE data management centers. This research was funded by a grant from the National Science Foundation. We thank D. Anderson, Y. Fialko, and M. Gurnis for helpful discussions. This is contribution number 8687 of the Division of Geological and Planetary Sciences at California Institute of Technology.

23 August 1999; accepted 9 November 1999

A Lower Mantle Source for Central European Volcanism

Saskia Goes,*† Wim Spakman, Harmen Bijwaard

Cenozoic rifting and volcanism in Europe have been associated with either passive or active mantle upwellings. Tomographic images show a low velocity structure between 660- and 2000-kilometer depth, which we propose to represent a lower mantle upwelling under central Europe that may feed smaller upper-mantle plumes. The position of the rift zones in the foreland of the Alpine belts and the relatively weak volcanism compared to other regions with plume-associated volcanism are probably the result of the past and present subduction under southern Europe.

The processes responsible for the formation of the Cenozoic system of rifts in central and western Europe are enigmatic. The rifts form an almost continuous system of extensional structures (Fig. 1) starting in the Valencia Trough [and possibly even further south in north Africa (*1*)], continuing through the Gulf of Lion and the Saône, Limagne, and Bresse grabens in France and the Rhine and Leine grabens in Germany and then bifurcating west into the Lower Rhine Embayment in the Netherlands and east into the Eger graben in the Bohemian Massif and into Poland.

Extensional activity along the European rift system started in the Eocene more or less contemporaneous with the main and late orogenic phases in the Alps in a belt around the Alpine collision front (*1*). Rifting was accompanied by localized volcanism and uplift possibly due to thermal doming. In several regions of the rift system, minor phases of older, pre-rifting volcanism have been dated (*2*). Seismicity defines zones of active extension in the Rhenish Massif, the lower Rhine Embayment, and the Massif Central (*3*). Active uplift (*1*, *4*) and volcanism only a few thousands years old (*2*) are documented in the Rhenish Massif, Massif Central, and parts of the Bohemian Massif. In

Vening Meinesz Research School of Geodynamics, Utrecht University, Post Office Box 80.021, 3508 TA Utrecht, Netherlands.

*To whom correspondence should be addressed. E-mail: saskia@tomo.ig.erdw.ethz.ch

†Present address: Institut für Geophysik, ETH Hönggerberg, 8093 Zurich, Switzerland.

the southern Rhine graben and the French grabens, extensional activity has ceased in the Miocene (*1*). The location of volcanism and faulting appears to be largely controlled by preexisting tectonic structures (*1*).

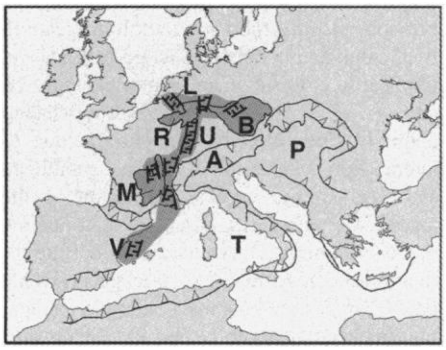

Fig. 1. On a tectonic map the approximate area covered by the European Cenozoic rift system is shaded. A, Alps; B, Bohemian Massif (includes the Eger graben in the north); L, Lower Rhine Embayment; M, Massif Central (cut by the Limagne graben in the north and bordered by the Saône and Bresse grabens in the east and the Gulf of Lion in the south); P, Pannonian Basin; R, Rhenish Massif; T, Tyrrhenean Sea; U, (Upper) Rhine Graben; and V, Valencia Trough. The sawtooth pattern represents thrust faults, and the hachured lines represent rift grabens.

The scale of the European Cenozoic rift system has led to the search for a common, plate scale mechanism. The end member hypotheses are (i) foreland splitting and passive upwelling due to the indentation of the Adriatic block (*5*) or due to plate scale extension (*1*) and (ii) rifting and volcanism in response to the presence of active mantle upwellings under the region (*6–9*). Although some regional extension may be occuring parallel to the Alpine arc, there are no indications that western and central Europe are experiencing a large-scale extensional stress regime or were under large-scale extension during the Cenozoic (*3*, *10*). Thus, it is difficult to explain the formation of the rift system and its continued activity as the result of indentation or plate boundary forces alone.

The existence of one or more mantle upwellings under Europe has been suggested based on geochemical and tomographic evidence. Geochemical studies (*7*, *8*, *11*) found a common mantle component in the rocks from the widely distributed European volcanic centers, including those from the Cenozoic rift system, the Canary Islands, and the back-arc Pannonian and Tyrrhenian basins. This component is different from normal asthenospheric mantle and has isotopic and incompatible element signatures similar to those of ocean island basalts (*7*, *8*, *11*), which are usually associated with mantle plumes. There is, however, no agreement on the upper or lower mantle origin of this component (*7*, *8*, *11*, *12*). Tomographic studies on various scales have imaged anomalously low velocities under central and western Europe (*7*, *8*, *13*, *14*). None of these velocity models has resolved structure below the upper mantle and a common root zone in either upper or lower mantle has not been identified. We use the tomographic model of Bijwaard *et al.* (*15*) to identify a possible lower mantle root for the European volcanic centers.

At depths down to about 400 km, the upper mantle structure under Europe contains several prominent low velocity anomalies (Fig. 2A). The low velocities below the Pannonian and western Mediterranean basins can be interpreted in the context of their back arc setting as the mantle wedge overlying the slab, possibly containing volatiles that produce the low velocities. Below 500- to 550-km depth, these basins are underlain by high velocity anomalies associated with subducted material (*13*, *16*) lying on the 660-km discontinuity (Fig. 2B). The low velocities under the Rhenish Massif and Massif Central have been attributed to small-scale up-

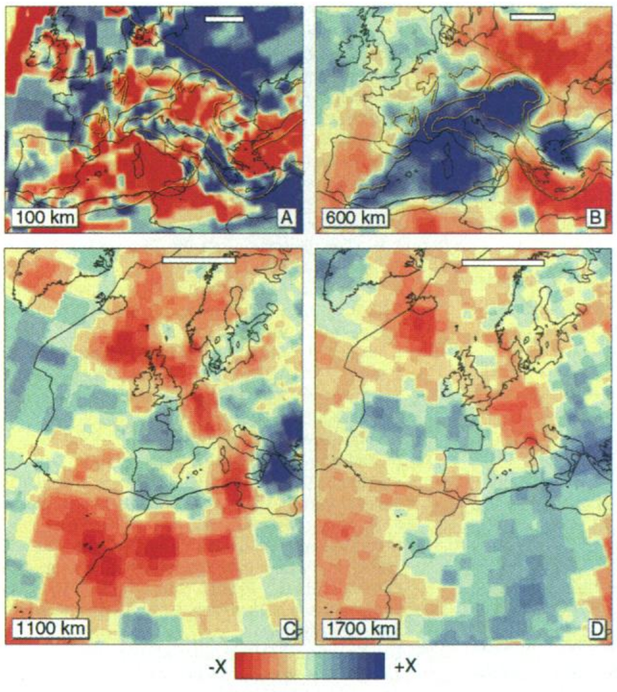

Fig. 2 (left). Tomographic images of *P* wave velocity anomalies represented as deviations from a one-dimensional reference model [AK135 (*27*)]. Shown are upper mantle cross sections under Europe at (**A**) 100-km and (**B**) 600-km depth and lower mantle cross sections (**C**) at 1100-km depth and (**D**) 1700-km depth for a larger region including Iceland and northern Africa. The white scale bars represent 500 km in (A) and (B) and 1000 km in (C) and (D). Resolution tests can be found in Web figure 1. The color scale bar represents the percentage difference in velocity, with the red colors indicating velocities slower than the reference model velocity and the blue colors indicating faster relative velocities. The scale varies for each panel, such that X = 2% in (A), 1% in (B), and 0.5% in (C) and (D).

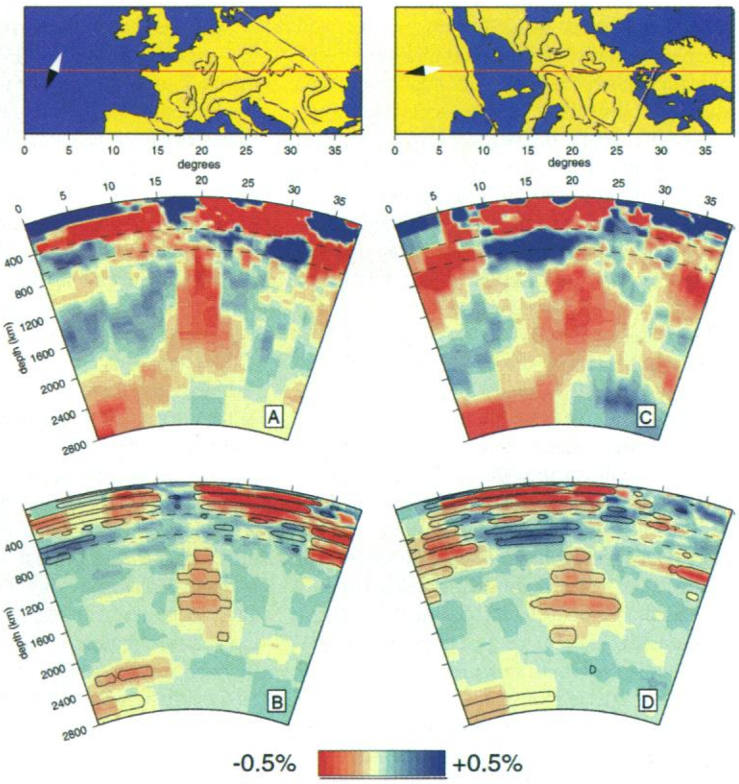

Fig. 3 (right). (**A**) and (**C**) are vertical cross sections through the *P* wave velocity model (represented as deviations from AK135; see Fig. 2 caption). Dotted lines mark the 400- and 660-km discontinuity. (**B**) and (**D**) show "layer cake" resolution tests (*15*). Thin black contours indicate the position of the input velocity anomalies (5% in the upper mantle and 0.5% in the lower mantle). In color the recovered structure is shown. The thin dashed lines mark the 410- and 660-km discontinuities.

per mantle upwellings (*8*). Many of the low velocity anomalies connect and skirt around the flat lying slabs under the western Mediterranean and the Pannonian basin (Fig. 2, A and B).

Within the transition zone (400- to 660-km depth), the low velocity anomalies under the Rhenish Massif and Massif Central disappear. The anomalies may have low amplitude, small dimensions, or both, but the detection of a continuation of the low velocity anomalies is hampered by the poor vertical resolution within the transition zone (Fig. 3). Granet and Trampert (*17*) imaged a low velocity anomaly beneath the Massif Central down to 800 km, but their resolution is poorer than that of the model shown here.

At the bottom of the transition zone, a low velocity anomaly under the Rhenish Massif starts to reappear and links up with a prominent lower mantle low velocity anomaly under central Europe (Fig. 3). In the shallow lower mantle (900- to 1200-km depth), the central European anomaly (CEA) is part of a semicircular low velocity structure that links the Iceland plume, the CEA, and a plume-like structure near the Canary Islands (Fig. 2C) that may continue down to the core-mantle boundary (*15*). Lower mantle low velocity anomalies under the Canary Islands connect to upper mantle low velocity anomalies under Spain. Note, however, that under northern Africa and the Atlantic Ocean, anomalies smaller than 300 km are not well resolved laterally. Below 1200 to 1300 km the semicircular structure separates into three anomalies again (Fig. 2D). The CEA continues down to 2000-km depth. Below 2000 km the structure may link up with a low velocity zone above the core-mantle boundary (CMB) located on the southwestern edge of the CEA, but the connection is not resolved. The CEA between 660 and 2000 km is well resolved laterally (Web figure 1, C and D), but some vertical smearing of the anomalies is observed (Fig. 3). The width of the anomaly in east-west direction is about 400 km and it is 1.5 to 2 times as long in north-south direction. The size is within the range predicted for the lower mantle from numerical models (*18*) and is similar in width to the low velocity anomaly interpreted as the lower mantle Iceland plume (*19*). With a lower spatial resolution the CEA is also present in the *S* wave velocities (*20*) and in other global body wave models (*21*).

Seismic velocity anomalies in the shallow mantle under Europe have been predominantly attributed to thermal structure (*22*). The low velocities between 50- and 200-km depth indicate the presence of asthenosphere as shallow as 100 km and elevated temperatures (by 100° to 300°C) relative to the surroundings (*22*), but they do not present evidence for anomalously hot mantle (with temperatures 75° to 300°C above an average mantle adiabat) as expected for plumes (*23*). At 400-km depth temperatures responsible for the low velocity anomalies are estimated to be about 1650°C, about 100°C above a mantle adiabat. The maximum amplitude of the lower mantle CEA is 0.55%. Using Karato's (*24*) $\partial V_P/\partial T$ estimate, this would correspond to a maximum temperature anomaly of 200°C, if the low velocities are attributed solely to temperature. The *S* wave (*20*) CEA (maximum amplitude of 0.8%) yields a similar temperature estimate. This is a lower bound on the maximum temperature because the amplitude of the anomaly may be underestimated. The thermal anomaly is consistent with estimates for other lower mantle plumes (*23*).

Evidence for upper mantle plume structures under western and central Europe has been found before (*7*, *8*, *17*), and a common root zone for these upwellings has been proposed (*7*, *8*, *11*). We suggest that the lower mantle low velocity anomaly under central Europe is the common root for European volcanism, supplying the heat and probably also some material for the upper mantle upwellings. We attribute the absence of a more mature rifting zone and large-scale volcanism, such as seen for example in the East African rift zone, to the interaction of the plume with subducted material under southern Europe and the predominantly compressive European stress regime (*10*). The thin European lithosphere (100 km or less) with preexisting zones of weakness (*1*) and the stress field associated with the Alpine collision (*5*) may allow the relatively weak plumes to reach the surface.

The ages of European rift volcanism indicate that—assuming volcanism is related to a lower mantle plume—the plume dates back to before subduction in the Mediterranean and Pannonian basins was fully developed [possibly as far back as the breakup of Pangea (*9*, *25*)]. In the upper mantle the upwelling plume material would have been progressively pushed aside by the subduction of cool material, forcing hot material to well up in a zone surrounding the subduction zones (Fig. 2B). This would be consistent with the observed synchronicity of Alpine orogenesis and western and central European rifting (*1*) and the geometry of the rifting zones in the foreland of the Alpine and Pannonian subduction zones. Furthermore the rifts closest to the Alpine front (Bresse, Saône, and upper Rhine grabens) have ceased their activity possibly in response to the advancing collision front, while the zones furthest away (Massif Central, Rhenish Massif, and northern Bohemian Massif) are still active or have been until very recently (*1*). Volcanism in the back-arc regions in the Pannonian and Tyrrhenian basins may tap an upper mantle previously affected by plume activity, explaining the plume signature seen in rocks from these regions (*7*) where volcanism is subduction-related. A lower mantle upwelling south of the Canary Islands may contribute to volcanism in the western Mediterranean.

The proposed scenario is consistent with numerical models (*26*) which show that lower mantle plumes trigger much narrower upper mantle plumes (possibly including some material exchange across 660 km) and that lateral displacement of upwelling material in the upper and shallow lower mantle may occur below downwellings. The seismic detection of upwellings in the transition zone may be hampered by their small width, and possibly also by their low amplitude caused by the interaction between the upwellings and the nearby cold subducted material (Figs. 2B and 3). The observed partial ring-shaped anomaly (Fig. 2C) may in part be due to lateral flow below the flat lying subducted slabs (given the vertical resolution of the model, the partial ring structure starts below the slab anomalies). Although neither the tomography presented here nor geochemical data (*7*, *8*, *11*) are conclusive about a connection between upper and lower mantle upwellings beneath central Europe, a lower mantle root and the interaction of upwelling material with subducted slabs provides a reasonable geodynamical explanation for European volcanism that is consistent with geological, seismological, and geochemical observations.

References and Notes

1. P. Ziegler, *Tectonophysics* **208**, 91 (1992).
2. J. Ulrych and E. Pivec, *Chem. Erde* **57**, 311 (1997); H. J. Lippolt, *Geol. Jahrb.* **D52**, 113 (1982); H. Downes, in *Alkaline Igneous Rocks*, J. G. Fitton and B. G. J. Upton, Eds., *Geol. Soc. Am. Spec. Publ.* **30**, 517 (Blackwell Scientific, Oxford, 1987).
3. L. Ahorner, B. Baier, K. P. Bonjer, in *Plateau Uplift: The Rhenish Shield—A Case History*, K. Fuchs *et al.*, Eds., (Springer-Verlag, Berlin, 1983), pp. 187–197; B. Müller *et al.*, *J. Geophys. Res.* **97**, 11,783 (1992).
4. H. Mälzer, in *Proceedings 3rd Workshop on the European Geotraverse (EGT) Project—The Central Segment*, R. Freeman, S. Müller, G. Calcagnile, Eds., (European Science Foundation, Strasbourg, 1986), pp. 249–254; H. Mälzer, G. Hein, K. Zippelt, in *Plateau Uplift: The Rhenish Shield—A Case History*, K. Fuchs *et al.*, Eds., (Springer-Verlag, Berlin, 1983), pp. 164–176.
5. J. H. Illies, *Tectonophysics* **29**, 251 (1975); A. M. C. Sengör, *Geology* **4**, 779 (1976).
6. R. A. Duncan, N. Petersen, R. B. Hargraves, *Nature* **239**, 82 (1972); C. Froidevaux, R. Brousse, H. Bellon, *Nature* **248**, 749 (1974).
7. K. Hoernle, Y. Zhang, D. Graham, *Nature* **374**, 34 (1995).
8. M. Granet, M. Wilson, U. Achauer, *Earth Planet. Sci. Lett.* **136**, 281 (1995).
9. R. Oyarzun *et al.*, *Geology* **25**, 727 (1997).
10. M. Gölke and D. Coblentz, *Tectonophysics* **266**, 11 (1996); G. Grünthal and D. Stromeyer, *J. Geophys. Res.* **97**, 11,805 (1992); J. J. P. Loohuis, M. J. R. Wortel, P. Th. Meijer, *Geophys. Res. Abs.* **1**, 85 (1999).
11. M. Wilson and H. Downes, *Tectonophysics* **208**, 173 (1992); M. Wilson, J. M. Rosenbaum, E. A. Dunworth, *Contrib. Mineral. Petrol.* **119**, 181 (1995); K. H. Wedepohl and A. Baumann, *Contrib. Mineral. Petrol.* **136**, 225 (1999).
12. Low European $^3He/^4He$ ratios (*29*) have been used as an argument against a lower mantle source (*7*). However, not all hot-spot volcanism has high $^3He/^4He$ [for example, B. B. Hanan and D. W. Graham, *Science* **272**, 991 (1996)], and tomographic (*21*) and geodynamical models have challenged the assumption of the lower mantle as a primitive (high $^3He/^4He$) reservoir [for example, P. J. Tackley *et al.*, *Nature*, **361**, 699 (1993); P. E. van Keken and C. J. Ballentine, *J. Geophys. Res.* **104**, 7137 (1999)].
13. W. Spakman, S. van der Lee, R. D. van der Hilst, *Phys. Earth Planet. Int.* **79**, 3 (1993).
14. A. Zielhuis and G. Nolet, *Geophys. J. Int.* **117**, 695 (1994); H. Marquering and R. Snieder, *Geophys. J. Int.* **124**, 283 (1996); S. Raikes and K. P. Bonjer, in *Plateau*

Uplift: The Rhenish Shield—A Case History, K. Fuchs *et al.*, Eds. (Springer-Verlag, Berlin, 1983), pp. 315–331.

15. H. Bijwaard, W. Spakman, E. R. Engdahl, *J. Geophys. Res.* **103**, 30,055 (1998). The global mantle velocity model of Bijwaard *et al.* is based on the *P*, *pP*, and *pwP* travel time data set of E. R. Engdahl *et al.* [*Bull. Seismol. Soc. Am.* **88**, 722 (1998)] and is computed using an irregular cell parameterization which adapts cell sizes to minimize ray sampling differences between adjacent cells. Under most of Europe, grid cells are 60 to 120 km in size. Cell size increases up to 300 km under the Atlantic and northern Africa. The tomographic model is supported by synthetic tests of the spatial resolution. So called "spike" tests [W. Spakman and G. Nolet, in: *Mathematical Geophysics: A Survey of Recent Developments in Seismology and Geodynamics*, N. J. Vlaar *et al.*, Eds. (Reidel, Dordrecht, Netherlands, 1988)] were computed for a range of "spike" sizes between 0.6° and 6° to determine the image resolution at different spatial scales. "Layer cake" tests used synthetic input models derived from the structures recovered in the tomographic model to test lateral and vertical resolution of the recovered features.
16. E. Carminati *et al.*, *Earth Planet. Sci. Lett.* **160**, 651 (1998).
17. M. Granet and J. Trampert, *Geophys. J. Int.* **99**, 583 (1989).
18. In the upper mantle plume conduits are thought to be very narrow (50 to 300 km) (*28*), while lower mantle plumes are thought to be significantly wider (around a factor of 3 to 5 times wider than upper mantle plumes) (*26*) because of the higher viscosity of the lower mantle.
19. H. Bijwaard and W. Spakman, *Earth Planet. Sci. Lett.* **166**, 121 (1999).
20. H. Bijwaard, thesis, Utrecht University, Netherlands (1999).
21. S. Grand, R. D. van der Hilst, S. Widiyantoro, *GSA Today* **7**, 1 (1997); R. D. van der Hilst, S. Widiyantoro, E. R. Engdahl, *Nature* **386**, 578 (1997).
22. S. Goes, R. Govers, P. Vacher, *J. Geophys. Res.*, in press.
23. The excess temperatures of plumes have been estimated to be 75 to 300°C in the upper mantle and 150 to 300°C in the lower mantle (*19*, *28*).
24. S. Karato, *Geophys. Res. Lett.* **20**, 1623 (1993).
25. D. L. Anderson, *Nature* **297**, 391 (1982).
26. P. E. van Keken and C. W. Gable *J. Geophys. Res.* **100**, 20,291 (1995); V. Steinbach and D.A. Yuen, *Phys. Earth Planet. Int.* **103**, 85 (1997); T. Nakakuki, D. A. Yuen, S. Honda, *Earth Planet. Sci. Lett.* **146**, 379–391, (1997); D. A. Yuen, L. Cserepes, B. A. Schroeder, *Earth Planets Space* **50**, 1035 (1998); B. Steinberger and R. J. O'Connell, *Geophys. J. Int.* **132**, 412 (1998).
27. B. L. N. Kennett, E. R. Engdahl, R. Buland, *Geophys. J. Int.* **122**, 108 (1995).
28. R. White and D. McKenzie, *J. Geophys. Res.* **94**, 7685 (1989); N. H. Sleep, *J. Geophys. Res.* **95**, 6715 (1990); G. Ito, J. Lin, C.W. Gable, *Earth Planet. Sci. Lett.* **144**, 53 (1996); H-C. Nataf and J. C. VanDecar, *Nature* **364**, 115 (1993); J. C. VanDecar, D. E. James, M. Assumpção, *Nature* **378**, 25 (1995); C. J. Wolfe *et al.*, *Nature* **385**, 245 (1997); Y. Shen *et al.*, *Nature* **395**, 62 (1998).
29. E. Griesshaber, R. K. O'Nions, E. R. Oxburgh, *Chem. Geol.* **99**, 213 (1992); T. J. Dunai and H. Baur, *Geochim. Cosmochim. Acta* **59**, 2767 (1995).

30. We thank M. Rehkämper for discussions on the geochemical signature of plumes and two reviewers for their critical reading of our manuscript. Funding was provided by the NEESDI program (NWO grant 750-29-601) (S.G.) and the Netherlands Geoscience Foundation (GOA) (H.B.), both financially supported by the Netherlands Organization for Scientific Research (NWO), and by the Vening-Meinesz Research School of Geodynamics.

12 August 1999; accepted 27 October 1999

Transition States Between Pyramids and Domes During Ge/Si Island Growth

F. M. Ross,* R. M. Tromp, M. C. Reuter

Real-time observations were made of the shape change from pyramids to domes during the growth of germanium-silicon islands on silicon (001). Small islands are pyramidal in shape, whereas larger islands are dome-shaped. During growth, the transition from pyramids to domes occurs through a series of asymmetric transition states with increasing numbers of highly inclined facets. Postgrowth annealing of pyramids results in a similar shape change process. The transition shapes are temperature dependent and transform reversibly to the final dome shape during cooling. These results are consistent with an anomalous coarsening model for island growth.

The formation of self-assembled islands, or quantum dots, during the epitaxial growth of Ge on Si is characterized by several distinct island shapes and an unusual island size distribution. The islands form spontaneously as a means of relieving the strain caused by the mismatch between the larger Ge lattice and the smaller lattice of the Si substrate. The question of whether the islands are thermodynamically stable or only transient structures is important both for understanding the general process of semiconductor epitaxy and for developing novel quantum dot–based electronic devices requiring well-controlled arrays of islands. Island growth has therefore been studied extensively using both in situ and post-growth analytical techniques.

For Ge deposition on Si(001), islands first appear after the formation of a flat wetting layer ~3 monolayers (ML) thick. At low growth temperatures the islands are rectangular-based huts with {501} facets (*1*), whereas at higher temperatures two different island shapes exist, depending on island size (*2*). Small islands are square-based pyramids, again with {501} facets, whereas larger islands are multifaceted domes, which have a higher aspect ratio and include facets such as {113} (*3*). The same island morphology is observed, although with larger lateral dimensions, for lower-strained Ge_xSi_{1-x} alloys on Si(001) (*4*).

Detailed observations of island shapes and size distributions made using scanning tunneling microscopy (*2, 5*) reveal interesting details of the evolution of the islands. Over a wide range of growth conditions, Ge islands show a bimodal distribution of sizes, with pyramids occupying the lower peak of the volume distribution and domes occupying the higher peak. Several models have been proposed (*2, 5, 6*) to explain how islands grow from low-volume pyramids to high-volume domes, and there is still much debate about which factors determine the island size distribution.

The details of the process that takes place as an island changes from a pyramid to a dome are crucial in understanding growth kinetics and in distinguishing between models. We have therefore studied island growth using low-energy electron microscopy (LEEM), a technique capable of distinguishing between different shapes and determining island sizes in real time during growth.

Our experiments were carried out in a LEEM apparatus with in situ growth capabilities, a base pressure of 2×10^{-10} torr, and a point resolution of 5 nm (*7*). Si(001) specimens were flash-cleaned and heated to the desired growth temperature of ~650° to 700°C. Ge_xSi_{1-x} was grown by chemical vapor deposition using a mixture of disilane and digermane gases introduced to the specimen area through a capillary tube. Typical growth rates, measured from the motion of steps in the early stages of growth or from post-growth cross-sectional analysis, were ~1 to 5 ML/min. Images were recorded at video rate, at electron energies of 5 to 10 eV.

In the LEEM images (Fig. 1A), pyramids are clearly distinguished by their cross-shaped pattern, whereas domes appear qualitatively different, most notably showing four bright areas each bisected by a narrow dark line. The eight bright regions, or facet beams, are only visible within a certain range of electron energy. They are formed when electrons diffracted from highly inclined facets pass through the objective aperture, and they indicate that additional facets are present on the domes; however, because of local focusing effects, the bright regions on the image may not correspond exactly to the spatial positions of the additional facets. Examination by ex situ scanning electron microscopy (Fig. 1B)

IBM T. J. Watson Research Center, Post Office Box 218, Yorktown Heights, NY 10598, USA.

*To whom correspondence should be addressed. E-mail: fmross@us.ibm.com

LINKED CITATIONS

You have printed the following article:

A Lower Mantle Source for Central European Volcanism
Saskia Goes; Wim Spakman; Harmen Bijwaard
Science, New Series, Vol. 286, No. 5446. (Dec. 3, 1999), pp. 1928-1931.
Stable URL:
http://links.jstor.org/sici?sici=0036-8075%2819991203%293%3A286%3A5446%3C1928%3AALMSFC%3E2.0.CO%3B2-8

This article references the following linked citations:

References and Notes

[12] **Lead and Helium Isotope Evidence from Oceanic Basalts for a Common Deep Source of Mantle Plumes**
B. B. Hanan; D. W. Graham
Science, New Series, Vol. 272, No. 5264. (May 17, 1996), pp. 991-995.
Stable URL:
http://links.jstor.org/sici?sici=0036-8075%2819960517%293%3A272%3A5264%3C991%3ALAHIEF%3E2.0.CO%3B2-O

NOTE: *The reference numbering from the original has been maintained in this citation list.*